Joint Time-Frequency Diversity in the Context of Spread-Spectrum Systems

Qiuhan Teng[1,2], Xuejun Sha[1(✉)], and Cong Ma[1]

[1] Harbin Institute of Technology, Harbin 150001, Heilongjiang, China
shaxuejun@hit.edu.cn
[2] The 54th Research Institute of China Electronics Technology Group Corporation, Shijiazhuang, China

Abstract. We discuss a new method for realizing the diversity in spread-spectrum communications over fast-fading multipath channels. Maximum Ratio Combining (MRC) can add the synchronized tributary signals in the weighted approach to obtain the maximum diversity gain. The signal distortion caused by the Doppler shift broadened spectrum cannot be eliminated. The diversity receiver used in existing systems suffers from significant performance degradation due to the rapid channel variations encountered under fast fading. We show that the Doppler spread caused by temporal channel variations actually provides other versatile means that can be further utilized to resist fading. This paper proposes a receiving method based on time-frequency cooperative processing. Joint time-frequency representation is a powerful tool. With precise synchronization and channel estimation, even the relatively small Doppler spread encountered in practice can be used for significant diversity gains by our approach. The framework is suitable for multiple mobile wireless multiple access systems and can provide significant performance improvements over existing systems.

Keywords: Time-frequency representation · Diversity · Doppler · Fast-fading · Multipath

1 Introduction

The signal fading caused by the channel causes the power of the received signal to fluctuate, and the performance of the receiver is significantly reduced, which is a major factor limiting improvements of wireless communication systems. Diversity is used to mitigate the degradation of error performance caused by unstable fading of the wireless channel. Its main idea is to transmit the same data over multiple independent fading paths. Since the probability of the independent path experiencing deep fading at the same time is small, the degree of fading of the received signal is reduced after proper merging.

After obtaining signals over multiple independent paths at the receiving end, branch signals which have been adjusted the phase and delay are weighted and linearly added to obtain the maximum gain. Three basic combination methods are formed owing to the different selection of weighting factors: selection combining, maximum ratio

S. Han et al. (Eds.): AICON 2019, LNICST 286, pp. 94–107, 2019.
https://doi.org/10.1007/978-3-030-22968-9_9

combining and equal gain combining. Among them, the maximum ratio combining method is the most effective. However, the increased mobility of cellular users leads to the fast fading of channel. The Doppler shift makes the spectrum of the signal broaden, which cannot be eliminated by maximum ratio combining [1].

Therefore, this paper proposes a diversity receiving method based on time-frequency cooperative processing. Joint time-frequency representation (TFR) is a powerful tool for processing time-varying signals and fast fading channels. With precise synchronization and channel estimation, this method can still produce significant gains even with relatively small Doppler spread.

2 Preliminaries

2.1 Time-Frequency Representation

Time-frequency representation (TFR) is a powerful tool for analyzing time-varying signals and time-varying systems. It processes non-stationary signals by blocking the time domain, and obtains two-dimensional signals that are parameterized by time and frequency. TFR is well suited for processing signals transmitted over time-varying channels and is also suitable for processing time-varying channels themselves [2].

A typical time-frequency analysis algorithm is the short-time Fourier transform (STFT) proposed by Gabor in 1946 [3]. Fourier transform (FT) is the basic tool of analysis in the frequency domain. The signal is multiplied by the time-limited window function before the Fourier transform, assuming that the non-stationary signal is stationary in the duration of the window function. By moving the window function on the time axis, multiple sets of partial spectrum of the signal can be obtained. By analyzing the difference between partial spectrum at different times, the time-varying characteristics of the signal can be obtained.

The TFR selected in this paper is the STFT which is defined for a signal $r(t)$ as

$$STFT_r(t,f) = \int_{-\infty}^{\infty} r(t')\eta^*(t'-t)e^{-j2\pi ft'}dt' \tag{1}$$

for a given window function $\eta(t)$ with a short time width.

2.2 Channel and Signal Models

Taking the spread spectrum signal in CDMA system as an example, the influence of Doppler shift on signal distortion is analyzed as follows. This paper assumes that in the case of single user, the spreading code used is M sequence. Under the premise of precise synchronization and channel estimation, inter symbol interference can be ignored.

The baseband signal $r(t)$ at the receiving end of one of the paths can be expressed as (see Fig. 1):

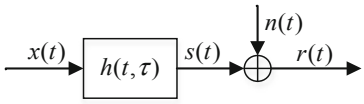

Fig. 1. Mobile wireless channel: linear time-varying system.

$$r(t) = s(t) + n(t) = \int_0^\infty h(t,\tau)x(t-\tau)d\tau + n(t) \tag{2}$$

where $h(t,\tau)$ is the channel function, and $n(t)$ is zero-mean, complex, circular AWGN with power spectral density N_0.

2.3 Fading and Diversity

Clarke proposed the Rayleigh channel model for describing the small-scale fading channel, which is a narrow-band channel statistical model. The statistical characteristics of the field strength of the transmitting signal and the received signal are based on scattering, which coincides with the characteristics of the shortwave channel. Therefore, it is widely used in channel modeling of shortwave channels [4]. In this paper, the Sum-Of-Sinusoid (SOS) method is taken as an example to study the characteristics of shortwave channels in the joint time-frequency domain.

Diversity is a way to overcome channel fading. It separates the received signals into uncorrelated multipath signals which carry the same information, and then combines and outputs the respective branch signals by combining techniques. Consequently, the probability of deep fading is greatly reduced at the receiving end.

Independent signals in multiple paths obtained by diversity at the receiving end can mainly adopt three different forms of combining techniques, which are maximum ratio combining (MRC), equal gain combining (EGC) and selective combining (SC) [5]. This article discusses the MRC approach, in which the weighting coefficients of each branch must match the channel. MRC achieves the best performance, maximizing the SNR after combining. As the number of receiving antennas increases, the performance of MRC is improved.

3 Joint Time-Frequency Diversity

The increasing mobility of cellular users makes the fast-fading characteristics of the channel more obvious, and consequently the Doppler shift broadens the original spectrum of the signal. MRC does not solve the problem of signal distortion caused by spectrum extension, so that additional techniques are required. In this paper, a time-frequency diversity receiving method is presented, which can further improve the performance by reducing the Doppler shift component on the basis of ensuring the diversity gain.

3.1 Time-Frequency Characteristics of Small-Scale Fading Channels

Assume that the carrier frequency of the signal in the channel is 10 MHz, the maximum Doppler shift is 200 Hz, the number of multipath is four, the delay is 0 ms, 1 ms, 3 ms and 5 ms respectively, and the loss power of each path is −6.96 dB, −6.49 dB, −4.70 dB, and −6.27 dB respectively, the path amplitude distribution and simulated time-frequency distribution characteristics of the channel are shown below (see Fig. 2 (a) and (b)).

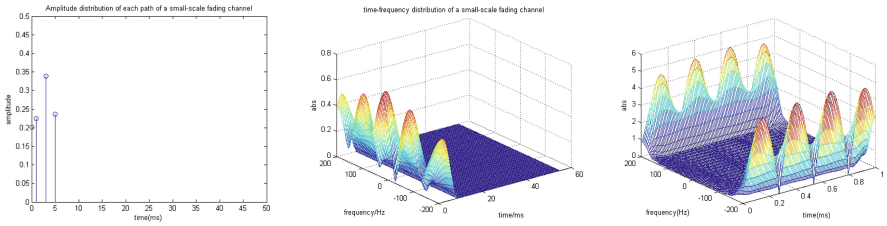

(a) (b) (c)

Fig. 2. Time-frequency distribution of small-scale fading channels.

In order to analyze the characteristics of the multipath channel, multiple mixed paths are separated. The time-varying spectrum and the time-varying power spectrum of the fast-fading channel of the single path in the time-frequency domain are given. A reasonable length of the time window and the frequency window are set in the optimal region. The window function is uniformly set to the Hamming window and the time window length of STFT is set to Odd(N/4), where N is the number of sampling points, and Odd means taking an odd number to obtain a better time-frequency resolution. The time-frequency diagram of the narrowband channel is obtained through simulation (see Fig. 2(c)).

The partial channel in the time window can be regarded as non-time-varying in joint time-frequency domain although the channel is always time-varying. Diversity is performed in units of time window to reduce the influence of fast-fading on the signal, which lays a foundation for the proposed diversity receiving method based on time-frequency cooperative processing.

3.2 Frequency Diversity

After complete synchronization of each signal, the time domain expression of the output signal obtained by MRC is

$$y_{MRC}(n) = \sum_{i=1}^{N_R} h_i^*(n) r_i(n) \tag{3}$$

According to the convolution theorem in the frequency domain, the above equation is equivalent to

$$Y_{MRC}(\omega) = \frac{1}{2\pi} \sum_{i=1}^{N_R} H_i^*(\omega) * R_i(\omega) \tag{4}$$

When the Eq. (4) is realized by the circular convolution, it is possible to gain the same effect shown in the Eq. (3) by the MRC. In the fading channel, the spectrum through the channel is broadened due to the presence of Doppler shift. Moreover, all spectral components are preserved when using circular convolution (see Fig. 3(c)).

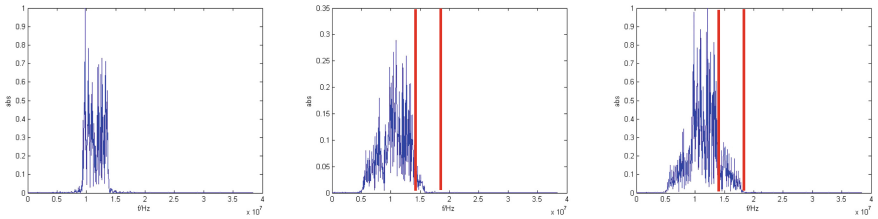

(a) (b) (c)

Fig. 3. Comparison chart of spectrum.

In order to weaken the influence of Doppler shift and further improve the performance of MRC, this paper proposes an improved method based on MRC. $H_i^*(\omega)$ and $R_i(\omega)$ are the FFT-transformed frequency domain sequences corresponding to the channel estimation conjugate sequence $h_i^*(n)$ and the received signal sequence $r_i(n)$ of one signal respectively. $H_i^*(\omega)$ and $R_i(\omega)$ are respectively shifted by 1/2 sequence length in the positive direction, and then linear convolution is used to implement Eq. (4).

After the linear convolution of each signal is completed, the results in frequency domain are obtained, which are recorded as $Y_i(\omega), \omega = 1, 2, 3, \cdots, 2N-1$. The first $N-1$ terms of $Y_i(\omega)$ is deleted, and $Y_i(\omega), \omega = N, N+1, \cdots, 2N-1$ are reserved as the frequency domain sequence of each signal after truncation (see Fig. 4(b)). Signals of all branches are combined after the above operations, and then the IFFT transform is conducted to obtain the time domain sequence.

It may be desirable to set the signal sequence received by one of the paths to $[r_1, r_2, r_3]$, the channel estimation conjugate sequence to $[h_1^*, h_2^*, h_3^*]$, and the corresponding FFT-transformed frequency domain sequence to be recorded as $[R_1, R_2, R_3]$ and $[H_1, H_2, H_3]$. See Appendix for the results of the linear convolution and truncation and the results of the circular convolution.

Comparing the results in Appendix with the spectrum information (see Fig. 3), it can be found that the above method can remove part of the high-frequency Doppler component away from the center frequency, that is, the area inside the red line in Fig. 3 (c). However, comparing Fig. 3(a) and (b), it is found that the truncation operation also

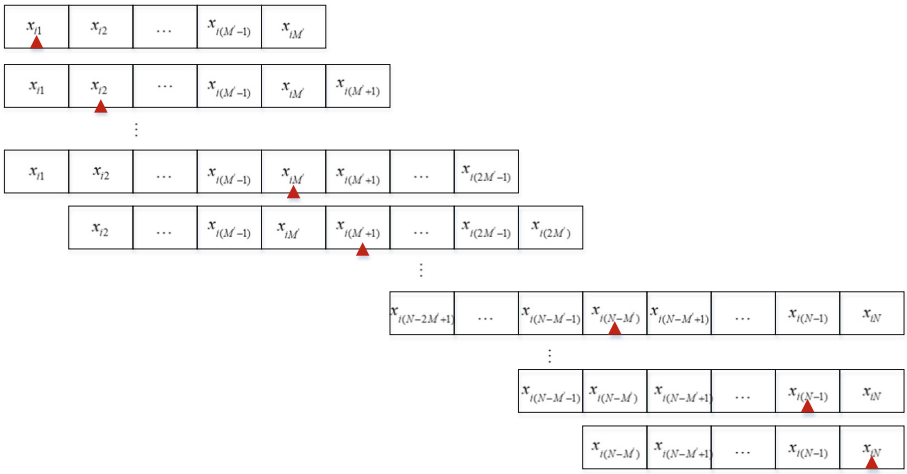

Fig. 4. Schematic diagram of the calculation process of STFT.

brings about partial distortion loss. In order to compensate for the distortion loss caused by the truncation operation, an attempt is made to implement the above method in the time-frequency domain.

3.3 Optimal Time-Frequency Receiver Structures

The frequency domain diversity and puncturing frequency operation described above can remove part of high-frequency Doppler components, which weakens the influence of the Doppler shift on MRC. However, linear convolution and truncation operations also introduce partial distortion loss to the signal. To compensate for the distortion loss of the signal, maximum ratio combining by STFT is proposed in this section. The operation of overlap, decomposition and addition of STFT can alleviate the distortion of the signal, and the window function can reduce the spectrum leakage.
The discrete form of STFT is

$$STFT_{r_i}(m,n) = \sum_{k=-\infty}^{\infty} r_i(k)g(k\Delta t - m\Delta t)e^{-j2\pi(n\Delta f)k}, n = \{1,2,\cdots,N\},\ m = \{1,2,\cdots,M\} \tag{5}$$

where $r_i(n)$ is a sampling sequence of a signal to be analyzed; $g(m)$ is the sampling sequence of the window function; N is the length of the sample sequence of the signal to be analyzed; M is the length of the sample sequence of the window function(odd), and $M' = (M+1)/2$.

The signal is segmented by the window function, and the sequence $x_i(n)$ to be analyzed is marked as $x_{in}g_m$ by elements obtained from segment of window function sequence $g(m)$ (see Fig. 4). $x_{i1}, x_{i2}, x_{i3}, \ldots\ldots, x_{iN}$ are considered as the center of the window in order, let the window slide, and then multiple groups of segment sequences

are gained. Figure 5 shows the case in which the moving step is a sequence element. The segment sequence is filled into the column elements of the original matrix by columns, and the missing column elements are zero-padded to obtain a total of N columns of elements (see Fig. 5). The N column element may contain all zero columns, depending on the moving step size when the window function slides. An N-point FFT is performed on each column element of the filled matrix to obtain a time-frequency distribution matrix after the STFT, and the matrix size is $N * N$.

$$\begin{bmatrix}
x_{i1}g_{M'} & x_{i2}g_{M'} & \cdots & x_{iM'}g_{M'} & x_{i(M'+1)}g_{M'} & \cdots & x_{i(N-M'+1)}g_{M'} & \cdots & x_{i(N-1)}g_{M'} & x_{iN}g_{M'} \\
x_{i2}g_{M'+1} & x_{i3}g_{M'+1} & \vdots & x_{i(M'+1)}g_{M'+1} & x_{i(M'+2)}g_{M'+1} & \vdots & x_{i(N-M'+2)}g_{M'+1} & \vdots & x_{iN}g_{M'+1} & 0 \\
x_{i3}g_{M'+2} & x_{i4}g_{M'+2} & \vdots & x_{i(M'+2)}g_{M'+2} & x_{i(M'+3)}g_{M'+2} & \vdots & x_{i(N-M'+3)}g_{M'+2} & \vdots & 0 & 0 \\
\vdots & \vdots & \vdots & \vdots & \vdots & \vdots & \vdots & \vdots & \vdots & \vdots \\
x_{i(M'-1)}g_{2M'-2} & x_{iM'}g_{2M'-2} & \vdots & x_{i(2M'-2)}g_{2M'-2} & x_{i(2M'-1)}g_{2M'-2} & \vdots & x_{i(N-1)}g_{2M'-2} & \vdots & 0 & 0 \\
x_{iM'}g_{2M'-1} & x_{i(M'+1)}g_{2M'-1} & \vdots & x_{i(2M'-1)}g_{2M'-1} & x_{i(2M')}g_{2M'-1} & \vdots & x_{iN}g_{2M'-1} & \vdots & 0 & 0 \\
0 & 0 & \vdots & 0 & 0 & \vdots & 0 & \vdots & 0 & 0 \\
0 & 0 & \vdots & 0 & 0 & \vdots & 0 & \vdots & 0 & 0 \\
\vdots & \vdots & \vdots & \vdots & \vdots & \vdots & \vdots & \vdots & \vdots & \vdots \\
0 & 0 & \vdots & 0 & 0 & \vdots & 0 & \vdots & 0 & 0 \\
0 & 0 & \vdots & x_{i1}g_1 & x_{i2}g_1 & \vdots & x_{i(N-2M'+2)}g_1 & \vdots & x_{i(N-M')}g_1 & x_{i(N-M'+1)}g_1 \\
0 & 0 & \vdots & x_{i2}g_2 & x_{i3}g_2 & \vdots & x_{i(N-2M'+3)}g_2 & \vdots & x_{i(N-M'+1)}g_2 & x_{i(N-M'+2)}g_2 \\
\vdots & \vdots & \vdots & \vdots & \vdots & \vdots & \vdots & \vdots & \vdots & \vdots \\
0 & 0 & \vdots & x_{i(M'-3)}g_{M'-3} & x_{i(M'-2)}g_{M'-3} & \vdots & x_{i(N-M'-2)}g_{M'-3} & \vdots & x_{i(N-4)}g_{M'-3} & x_{i(N-3)}g_{M'-3} \\
0 & 0 & \vdots & x_{i(M'-2)}g_{M'-2} & x_{i(M'-1)}g_{M'-2} & \vdots & x_{i(N-M'-1)}g_{M'-2} & \vdots & x_{i(N-3)}g_{M'-2} & x_{i(N-2)}g_{M'-2} \\
0 & x_{i1}g_{M'-1} & \vdots & x_{i(M'-1)}g_{M'-1} & x_{iM'}g_{M'-1} & \vdots & x_{i(N-M')}g_{M'-1} & \vdots & x_{i(N-2)}g_{M'-1} & x_{i(N-1)}g_{M'-1}
\end{bmatrix}$$

Fig. 5. Calculation matrix of STFT.

The time-frequency distribution matrix of each signal sample sequence $r_i(n)$ and channel estimation conjugate sequence $h_i^*(n)$ is calculated by STFT time-frequency analysis method, and is recorded as $R_i(t,\omega)$ and $H_i(t,\omega)$. The time-frequency distribution matrices $R_i(t,\omega)$ and $H_i(t,\omega)$ are linearly convoluted in columns. The convoluted matrix is denoted as $S_i(t,\omega)$, and the matrix size is $(2N-1) * N$.

Suppose the element of row k and column j of matrix $R_i(t,\omega)$ is $r_i^j(k)$, the element of row k and column j of matrix $H_i(t,\omega)$ is $h_i^j(k)$, the element of row k and column j of matrix $S_i(t,\omega)$ is $s_i^j(k)$, the convolution operation satisfies the following equation:

$$s_i^j(k) = \sum_{\tau=1}^{N} r_i^j(\tau) h_i^j(k-\tau) \tag{6}$$

The column element of matrix $S_i(t,\omega)$ is $s_i^j(n), n = 1,2,3,\cdots,2N-1$. The first $N-1$ of each column element $s_i^j(n), n = 1,2,3,\cdots,N-1$ is deleted and the remaining N elements $s_i^j(n), n = N, N+1,\cdots,2N-1$ are the truncated matrix column elements. The new matrix is denoted as S_{inew}.

The truncated convolution matrix S_{inew} gained by each operation is linearly superposed to obtain the matrix S_{sum}. The inverse short-time Fourier transform (ISTFT) of the matrix S_{sum} is applied to obtain the reconstructed time domain sequence $x_{re}(n)$ of the signal.

In summary, the steps of the diversity method of time-frequency coordinated processing can be summarized as follows (see Fig. 6):

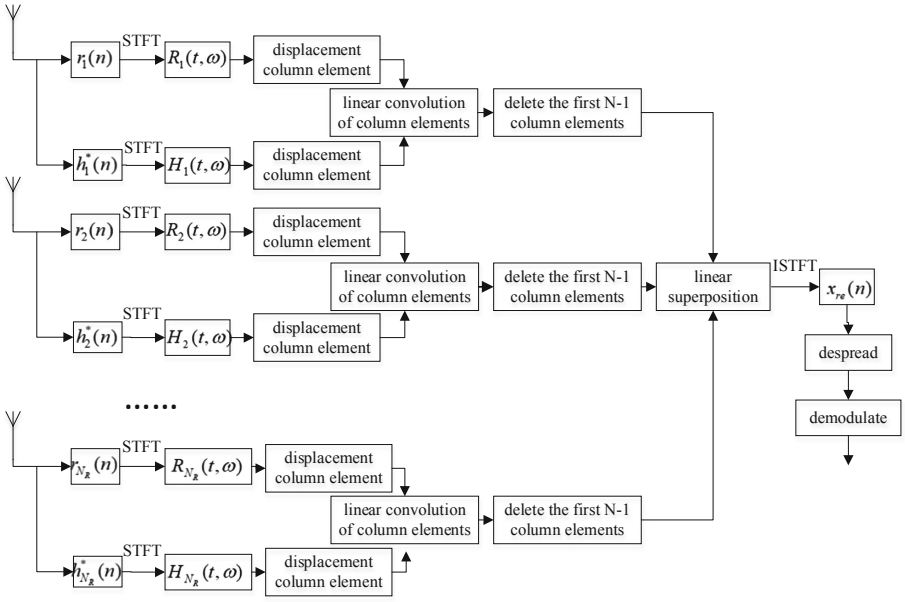

Fig. 6. Implementation flowchart.

(1) The multi-path signals received by the N antennas are subjected to synchronization processing and channel estimation to obtain multiple signals to be processed ($r_i(n)$) and channel estimation conjugate sequences ($h_i^*(n)$, $i = 1, 2, \cdots, N_R$). The lengths of $r_i(n)$ and $h_i^*(n)$ are both N;

(2) The time-frequency distribution matrix of $r_i(n)$ and $h_i^*(n)$ is calculated by STFT, which is denoted as $R_i(t, \omega)$ and $H_i(t, \omega)$. The matrix size is $N * N$;

(3) The column elements of the time-frequency distribution matrices $R_i(t, \omega)$ and $H_i(t, \omega)$ are circumferentially shifted by 1/2 sequence length in the positive direction. $R_i(t, \omega)$ and $H_i(t, \omega)$ are then linearly convolved in columns. The convoluted matrix is denoted as $S_i(t, \omega)$ and the matrix size is $(2N - 1) * N$. The first $N - 1$ terms of each column of matrix are deleted and the new matrix is denoted as S_{inew}. The matrix size is $N * N$;

(4) The truncated convolution matrix S_{inew} obtained from each path are linearly superposed to get the matrix S_{sum}. The matrix S_{sum} is subjected to an inverse short-time Fourier transform (ISTFT) to obtain a time domain sequence $x_{re}(n)$ of the reconstructed signal, which is to be demodulated.

4 Discussion

In this section, we present the practical feasibility and potential gains of the diversity receiving method based on joint time-frequency processing and determine the optimal window function overlap rate.

4.1 Potential Performance Gains

In order to test the superiority of the time-frequency diversity receiving method proposed in this paper in suppressing channel fading, several simulations are carried out. The transmission signal is set to QPSK modulated spread spectrum signal, the spreading code is M sequence of 7-bit, the carrier frequency is 11.52 MHz, the duration of each symbol is 0.26042e−6 s, and the sampling frequency is 38.4 MHz. This system contains signals over two paths and the Clarke channel model is selected. The simulations are performed on the premise of precise synchronization and channel estimation.

Comparing the time-frequency distributions of the signals, it can be found that without any noise in the channel, the time-frequency distribution of the signal is distorted after the fading of the channel. At the same time, due to the expansion of the Doppler shift, the spectrum of the signal is also broadened (see Fig. 7(a)). After the maximum ratio combining, the signal distortion turns to be suppressed, but the expansion of the Doppler spectrum has not been improved (see Fig. 7(b)). With the time-frequency diversity receiving method proposed in this paper, part of the Doppler shift is removed based on the performance obtained by the MRC, and the performance can be further improved (see Fig. 7(c)).

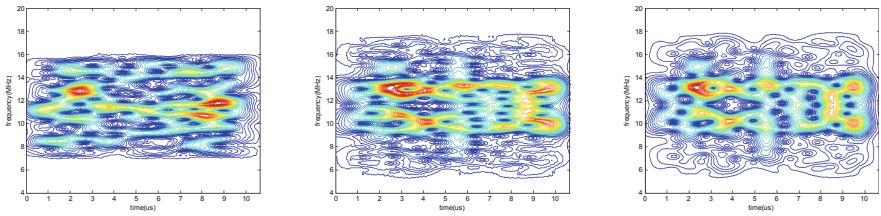

(a) (b) (c)

Fig. 7. Time-frequency distribution of each signal.

Using the bit error rate (BER) as the test index, the comparison of different methods is obtained. (see Fig. 8). It can be found that when MRC is implemented by linear convolution and the removal of partial Doppler shift, the BER increases due to large distortion loss. Nevertheless, with the method proposed in this paper, the distortion is alleviated, and partial Doppler shift is removed. Compared with MRC, the bit error rate can be further reduced and the performance can be further improved.

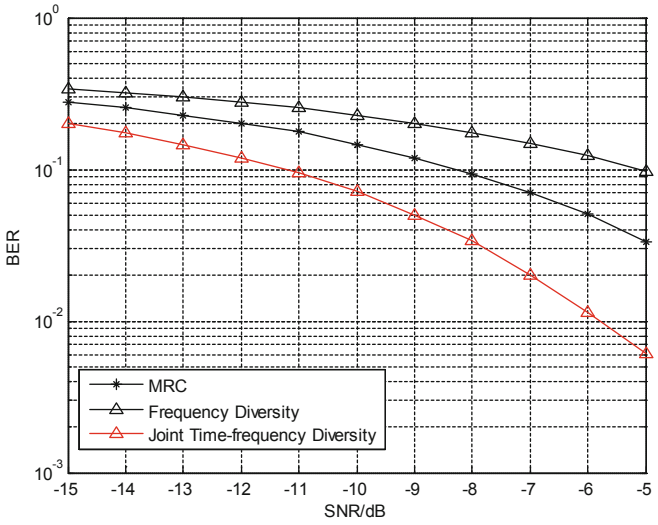

Fig. 8. BER-SNR

4.2 Optimal Window Function Parameter

It can be known from the Heisenberg uncertainty principle that a window function which has both the arbitrary small time width and the arbitrary small bandwidth does not exist. In order to get the best performance of the proposed method, it is necessary to find the optimal window function parameters. An important issue related to the process of the overlap segment is the degree of correlation between the segment sequences, which can be defined by a relatively flat noise power spectrum over the window bandwidth [6]. It is a function of the overlap rate r, which can be measured by

$$c(r) = \frac{\sum_{n=0}^{rN-1} g(n)g(n+(1-r)N)}{\sum_{n=0}^{N-1} g^2(n)} \tag{7}$$

When multiple independent measurements are conducted on K identical distribution variables, the relationship between the mean variance and the single variance of multiple measurements can be expressed by the following equation:

$$\frac{\sigma_{Avg}^2}{\sigma_{Mean}^2} = \frac{1}{K} \tag{8}$$

Thus, for the sequence after overlap truncation, Welch [6] gives another form of the above formula:

$$\begin{aligned}\frac{\sigma_{Avg}^2}{\sigma_{Mean}^2} &= \frac{1}{K}[1+2\cdot\frac{K-1}{K}\sum_{i=1,i\in N}^{ir-(i-1)>0} c^2(ir-(i-1))] \\ &= \frac{1-r}{L/N-r}\cdot[1+2\cdot(1-\frac{1-r}{L/N-r})\cdot\sum_{i=1,i\in N}^{ir-(i-1)>0} c^2(ir-(i-1))]\end{aligned} \tag{9}$$

It can be seen that $\sigma_{Avg}^2/\sigma_{Mean}^2$ varies with the length, type and overlap rate of the window function. Under the simulation conditions set in Sect. 4.1, the above three parameters are changed separately in the case of $SNR = -10dB$. It can be found that the BER hardly changes with the change of the window length. As the overlap rate increases, the BER decreases. When it increases continuously and reaches the optimal overlap rate, the BER begins to flatten and almost remains unchanged. When the window function is taken from the Hamming window, the rectangular window, the triangular window, the Gaussian window and the Blackman window, the optimal overlap ratio is 75%, 85%, 85%, 80% and 80%, respectively, all of which are about 80%.

5 Conclusion

In wireless mobile communication, the movement of the users leads to the intensified signal fading and the decrease of the receiving end performance. The MRC can add the synchronized tributary signals in the weighted approach to obtain the maximum diversity gain. However, the signal distortion caused by the Doppler shift can't be eliminated. In this paper, a time-frequency diversity receiving method is proposed. Each branch signal is analyzed in the time-frequency domain and weighted. Some high-frequency Doppler components are removed by truncation and subtraction, and the branches are combined by summation. The overlapping decomposition and averaging processing of the time-frequency analysis can reduce the effective noise bandwidth and alleviate the distortion loss caused by windowing and frequency clipping. In summary, the time-frequency diversity receiving method can obtain additional performance gain by suppressing the Doppler shift on the basis of ensuring the original performance gain of the MRC. As the overlap rate increases, the BER decreases. When it increases to 80% of the optimal overlap rate, the BER begins to flatten.

Declaration. This work is supported partially by the fund of Science and Technology on Communication Networks Laboratory under grand (No. SXX18641X027) and the National Natural Science Foundation General Program of China (No. 61671179).

Appendix

$$R_1 = r_1 + r_2 + r_3 \tag{10}$$

$$R_2 = r_1 + r_2 e^{-j\frac{2\pi}{3}} + r_3 e^{-j\frac{4\pi}{3}} \tag{11}$$

$$R_3 = r_1 + r_2 e^{-j\frac{4\pi}{3}} + r_3 e^{-j\frac{8\pi}{3}} \tag{12}$$

$$H_1 = h_1^* + h_2^* + h_3^* \tag{13}$$

$$H_2 = h_1^* + h_2^* e^{-j\frac{2\pi}{3}} + h_3^* e^{-j\frac{4\pi}{3}} \tag{14}$$

$$H_3 = h_1^* + h_2^* e^{-j\frac{4\pi}{3}} + h_3^* e^{-j\frac{8\pi}{3}} \tag{15}$$

The results obtained by circularly convolving sequences $[R_1, R_2, R_3]$ and $[H_1, H_2, H_3]$ are as follows:

$$\begin{aligned} R_3H_2 + R_1H_1 + R_2H_3 &= (r_1 + r_2 e^{-j\frac{4\pi}{3}} + r_3 e^{-j\frac{8\pi}{3}})(h_1^* + h_2^* e^{-j\frac{2\pi}{3}} + h_3^* e^{-j\frac{4\pi}{3}}) \\ &+ (r_1 + r_2 + r_3)(h_1^* + h_2^* + h_3^*) \\ &+ (r_1 + r_2 e^{-j\frac{2\pi}{3}} + r_3 e^{-j\frac{4\pi}{3}})(h_1^* + h_2^* e^{-j\frac{4\pi}{3}} + h_3^* e^{-j\frac{8\pi}{3}}) \\ &= 3r_1h_1^* + r_2h_1^* + r_3h_1^* + r_1h_2^* + r_2h_2^* + r_3h_2^* + r_1h_3^* + r_2h_3^* + r_3h_3^* \\ &+ (r_1h_2^* + r_2h_1^*)e^{-j\frac{2\pi}{3}} + (r_1h_2^* + r_2h_1^* + r_1h_3^* + r_3h_1^*)e^{-j\frac{4\pi}{3}} \\ &+ (r_3h_1^* + r_2h_3^* + r_3h_2^* + r_1h_3^*)e^{-j\frac{8\pi}{3}} + 2r_2h_2^*e^{-j2\pi} + 2r_3h_3^*e^{-j4\pi} \\ &+ (r_2h_3^* + r_3h_2^*)e^{-j\frac{10\pi}{3}} \end{aligned} \tag{16}$$

$$\begin{aligned} R_3H_3 + R_1H_2 + R_2H_1 &= (r_1 + r_2 e^{-j\frac{4\pi}{3}} + r_3 e^{-j\frac{8\pi}{3}})(h_1^* + h_2^* e^{-j\frac{4\pi}{3}} + h_3^* e^{-j\frac{8\pi}{3}}) \\ &+ (r_1 + r_2 + r_3)(h_1^* + h_2^* e^{-j\frac{2\pi}{3}} + h_3^* e^{-j\frac{4\pi}{3}}) \\ &+ (r_1 + r_2 e^{-j\frac{2\pi}{3}} + r_3 e^{-j\frac{4\pi}{3}})(h_1^* + h_2^* + h_3^*) \\ &= (r_1h_2^* + r_2h_1^* + r_1h_3^* + r_2h_3^* + 2r_3h_3^* + r_3h_2^* + r_3h_1^*)e^{-j\frac{4\pi}{3}} \\ &+ 3r_1h_1^* + r_2h_1^* + r_3h_1^* + r_1h_2^* + r_1h_3^* + r_3h_3^*e^{-j\frac{16\pi}{3}} \\ &+ (2r_2h_2^* + r_2h_3^* + r_3h_2^* + r_1h_2^* + r_2h_1^*)e^{-j\frac{2\pi}{3}} \\ &+ (r_1h_3^* + r_2h_2^* + r_3h_1^*)e^{-j\frac{8\pi}{3}} + (r_2h_3^* + r_3h_2^*)e^{-j4\pi} \end{aligned} \tag{17}$$

$$\begin{aligned}R_3H_1+R_1H_3+R_2H_2 &= (r_1+r_2e^{-j\frac{4\pi}{3}}+r_3e^{-j\frac{8\pi}{3}})(h_1^*+h_2^*+h_3^*)\\ &+(r_1+r_2+r_3)(h_1^*+h_2^*e^{-j\frac{4\pi}{3}}+h_3^*e^{-j\frac{8\pi}{3}})\\ &+(r_1+r_2e^{-j\frac{2\pi}{3}}+r_3e^{-j\frac{4\pi}{3}})(h_1^*+h_2^*e^{-j\frac{2\pi}{3}}+h_3^*e^{-j\frac{4\pi}{3}})\\ &=(r_2h_1^*+2r_2h_2^*+2r_2h_3^*+r_1h_2^*+r_2h_2^*+r_3h_2^*+r_1h_3^*+r_3h_1^*)e^{-j\frac{4\pi}{3}}\\ &+3r_1h_1^*+r_1h_2^*+r_1h_3^*+r_3h_1^*+2r_2h_1^*+r_1h_2^*e^{-j\frac{2\pi}{3}}+r_3h_2^*e^{-j2\pi}\\ &+(r_3h_1^*+r_3h_2^*+r_3h_3^*+r_1h_3^*+r_2h_3^*+2r_3h_3^*)e^{-j\frac{8\pi}{3}}\end{aligned} \tag{18}$$

The sequences $[R_1, R_2, R_3]$ and $[H_1, H_2, H_3]$ are circumferentially shifted by 1/2 sequence length in the positive direction to obtain sequences $[R_3, R_1, R_2]$ and $[H_3, H_1, H_2]$. The results of linear convolution of the sequences C and D and truncation are as follows:

$$\begin{aligned}R_3H_2+R_1H_1+R_2H_3 &= (r_1+r_2e^{-j\frac{4\pi}{3}}+r_3e^{-j\frac{8\pi}{3}})(h_1^*+h_2^*e^{-j\frac{2\pi}{3}}+h_3^*e^{-j\frac{4\pi}{3}})\\ &+(r_1+r_2+r_3)(h_1^*+h_2^*+h_3^*)\\ &+(r_1+r_2e^{-j\frac{2\pi}{3}}+r_3e^{-j\frac{4\pi}{3}})(h_1^*+h_2^*e^{-j\frac{4\pi}{3}}+h_3^*e^{-j\frac{8\pi}{3}})\\ &=3r_1h_1^*+r_2h_1^*+r_3h_1^*+r_1h_2^*+r_2h_2^*+r_3h_2^*+r_1h_3^*+r_2h_3^*+r_3h_3^*\\ &+(r_1h_2^*+r_2h_1^*)e^{-j\frac{2\pi}{3}}+(r_1h_2^*+r_2h_1^*+r_1h_3^*+r_3h_1^*)e^{-j\frac{4\pi}{3}}\\ &+(r_3h_1^*+r_2h_3^*+r_3h_2^*+r_1h_3^*)e^{-j\frac{8\pi}{3}}+2r_2h_2^*e^{-j2\pi}\\ &+2r_3h_3^*e^{-j4\pi}+(r_2h_3^*+r_3h_2^*)e^{-j\frac{10\pi}{3}}\end{aligned} \tag{19}$$

$$\begin{aligned}R_3H_1+R_1H_3 &= (r_1+r_2e^{-j\frac{4\pi}{3}}+r_3e^{-j\frac{8\pi}{3}})(h_1^*+h_2^*+h_3^*)\\ &+(r_1+r_2+r_3)(h_1^*+h_2^*e^{-j\frac{4\pi}{3}}+h_3^*e^{-j\frac{8\pi}{3}})\\ &=2r_1h_1^*+r_1h_2^*+r_1h_3^*+r_3h_1^*+r_2h_1^*\\ &+(r_2h_1^*+2r_2h_2^*+r_2h_3^*+r_1h_2^*+r_3h_2^*)e^{-j\frac{4\pi}{3}}\\ &+(r_3h_1^*+r_3h_2^*+r_3h_3^*+r_1h_3^*+r_2h_3^*+r_3h_3^*)e^{-j\frac{8\pi}{3}}\end{aligned} \tag{20}$$

$$\begin{aligned}R_3H_3 &= (r_1+r_2e^{-j\frac{4\pi}{3}}+r_3e^{-j\frac{8\pi}{3}})(h_1^*+h_2^*e^{-j\frac{4\pi}{3}}+h_3^*e^{-j\frac{8\pi}{3}})\\ &=r_1h_1^*+(r_1h_2^*+r_2h_1^*)e^{-j\frac{4\pi}{3}}+(r_2h_2^*+r_3h_1^*+r_1h_3^*)e^{-j\frac{8\pi}{3}}\\ &+(r_3h_2^*+r_2h_3^*)e^{-j4\pi}+r_3h_3^*e^{-j\frac{16\pi}{3}}\end{aligned} \tag{21}$$

References

1. Sayeed, A.M., Aazhang, B.: Joint multipath-Doppler diversity in mobile wireless communications. IEEE Trans. Commun. **47**(1), 123–132 (1999)
2. Boashash, B., Azemi, G., Khan, N.A.: Principles of time-frequency feature extraction for change detection in non-stationary signals: applications to newborn EEG abnormality detection. Pattern Recogn. **48**(3), 616–627 (2015)
3. Portnoff, M.: Time-frequency representation of digital signals and systems based on short-time Fourier analysis. IEEE Trans. Acoust. Speech Signal Process. **28**(1), 55–69 (2003)
4. Cho, Y.S.: MIMO-OFDM Wireless Communications with MATLAB. Wiley, Hoboken (2010)
5. Agrawal, D.P., Zeng, Q.A.: Introduction to Wireless and Mobile Systems, 4nd edn (2016)
6. Welch, P.D.: The use of fast Fourier transform for the estimation of power spectra: a method based on time averaging over short, modified periodograms. IEEE Trans. Audio Electroacoust. **15**(2), 70–73 (1967)